



Non-thermal emission from the reverse shock of the youngest galactic Supernova remnant G1.9+0.3



R. Brose^{1,2}, I. Sushch¹, M. Pohl^{1,2}

DESY, 15738 Zeuthen, Germany

Institute of Physics and Astronomy, University of Potsdam, 14476 Potsdam, Germany

Abstract

The youngest galactic Supernova remnant G1.9+0.3 is an interesting target for next generation gamma-ray observatories. So far the remnant is only detected in the radio and the X-ray bands but its young age and inferred shock speed of 14,000 km/s should make it an efficient particle accelerator. We explain the observed radio- and x-ray fluxes together with the morphology of the remnant. At the same time we are estimating the gamma-ray flux of the source and evaluate the prospects of its detection with future gamma-ray experiments. We carry out spherical symmetric 1-D simulations where we simultaneously solve the transport equations for the cosmic rays, the transport equation for magnetic turbulence and the hydro-dynamical flow using the RATPaC code. The separately obtained particle spectra for the acceleration at the forward and the reverse shock are then used to calculate the radio, x-ray, inverse Compton and Pion-decay radiation from the source. We are able to show that the emission from G1.9+0.3 can be explained with our self-consistent model. Furthermore is the observed morphology indicating, that the x-ray flux is dominated by emission from the forward shock while most of the radio-emission is originated at the reverse shock, which makes G1.9+0.3 the first remnant with non-thermal radiation detected from the reverse shock.

1. The modelling

We solve the time-dependent transport equation for **cosmic-rays** [1, 2, 3], for the transport of **Alfvénic turbulence** [4] and the standard **gas-dynamical equations** [5] in spherically-symmetric 1-D geometry under the test-particle assumption:

$$\frac{\partial N}{\partial t} = \nabla(D_r \nabla N - \vec{u}N) - \frac{\partial}{\partial p} \left((N\dot{p}) - \frac{\nabla \vec{u}}{3} N p \right) + Q \quad (1)$$

$$\frac{\partial E_w}{\partial t} + \vec{u} \cdot (\nabla E_w) + (\nabla \cdot \vec{u}) E_w + k \frac{\partial}{\partial k} \left(k^2 D_k \frac{\partial E_w}{\partial k} \right) = 2(\Gamma_g - \Gamma_d) E_w \quad (2)$$

$$\frac{\partial}{\partial t} \begin{pmatrix} \rho \\ \vec{m} \\ E \end{pmatrix} + \nabla \begin{pmatrix} \rho \vec{u} \\ \vec{m} \vec{u} + P \mathbf{I} \\ (E + p) \vec{u} \end{pmatrix} = \begin{pmatrix} 0 \\ 0 \\ 0 \end{pmatrix} \quad (3)$$

$$\frac{\rho \vec{u}^2}{2} + \frac{P}{\gamma - 1} = E \quad (4)$$

N Differential Number density of cosmic rays	\dot{p} Energy losses
p Particle momentum	Q Source of thermal particles
\vec{u} Advection velocity	D_k Diffusion coefficient in wave-number space
E_w Spectral energy density in Alfvénic turbulence	Γ Source and damping coefficients
k Wave-number	ρ Plasma density
\vec{m} Momentum density ($= \rho \vec{v}$)	P Plasma pressure
γ Adiabatic index of the Plasma	E Total energy of the Plasma

We initialise the simulation as a Type Ia-explosion following [6] with 10^{51} erg explosion energy and 1.4 solar masses of ejecta.

A ambient density of 0.03 cm^{-3} gives a forward-shock radius of 2.2 pc after 105 years and a shock speed of 14,000 km/s. The reverse shock radius would be 1.85 pc and the expansion speed 11,000 km/s.

3. The radio and x-ray morphology

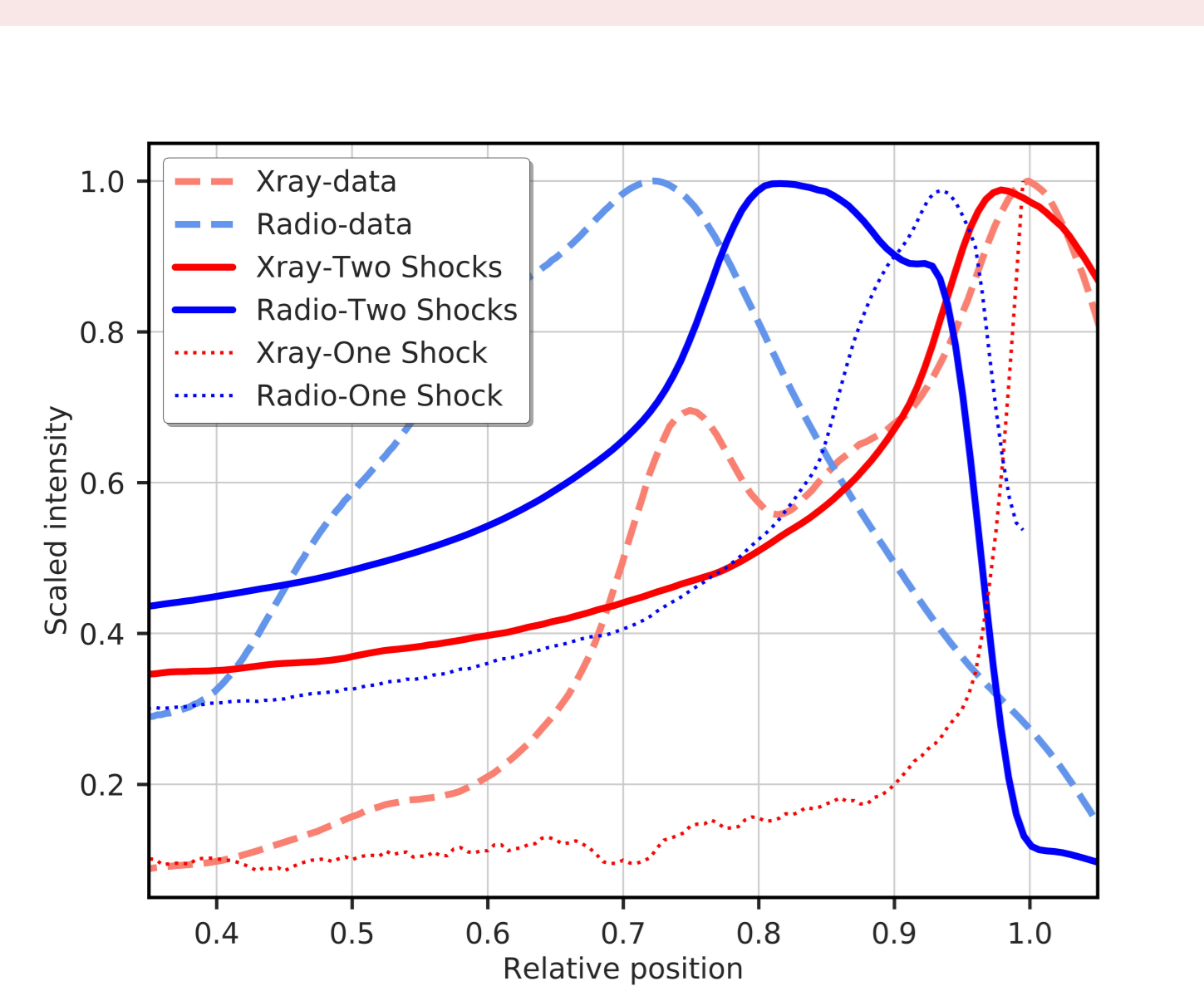


Figure: Morphology of the remnant in x-ray and radio. The x-ray data is taken from [7] and the radio-data is from Luken et al. (in preparation). We extracted the averaged profiles in the East-West direction from the 2D maps covering the x-ray ears. The same method was applied to the theoretical data.

The separation between the peaks of the x-ray and radio emission is about 25% in the East-West direction of G1.9+0.3. This separation is hard to match even with a two-shock model, as the reverse shock radius is about 84% of the forward shock radius. However, the separation we obtain for our two-shock model is about 20% and quite close to the value observed. In case of a one-shock scenario, the separation would be much smaller with about 6%.

This scenario further allows to explain the different morphologies of the x-ray and the radio emission of the remnant. As the bipolar x-ray structure might be caused by the orientation of the ambient magnetic field, this would not influence the acceleration at the reverse shock. An asymmetric explosion or an higher ambient density towards the north of the remnant would explain the morphology of the radio emission without affecting the x-ray emission.

6. Conclusions

In this work we studied the supernova remnant G1.9+0.3 through the modelling of its broadband non-thermal emission aiming to explain the observed spectral energy distribution, the morphology, the brightening rate at radio frequencies and the prospects for detecting the remnant with CTA. Therefore we solved the transport equations for cosmic rays and alfvénic turbulence together with the standard gas-dynamical equations and subsequently calculated the emission from the forward and the reverse shock under the assumption of spherical symmetry. We found that:

2. The non-thermal emission

We calculated the emission of the remnant through synchrotron (SY), Pion-decay (PD) and inverse-Compton (IC) radiation on CMB and IR-photons. The radio emission is dominated by emission from the reverse shock (RS), whereas the forward shock (FS) contributes most of the gamma-ray emission and all of the x-ray emission.

The peak magnetic field we obtain is $270 \mu\text{G}$ behind the forward shock and $60 \mu\text{G}$ behind the reverse shock, which both represent $\approx 0.3\%$ of the energy in the downstream plasma-flow. The field drops sharply behind both shocks due to fast turbulence damping through cascading. The cosmic-ray pressure stays well below 10% of the shock ram pressure at both shocks justifying our test-particle assumption.

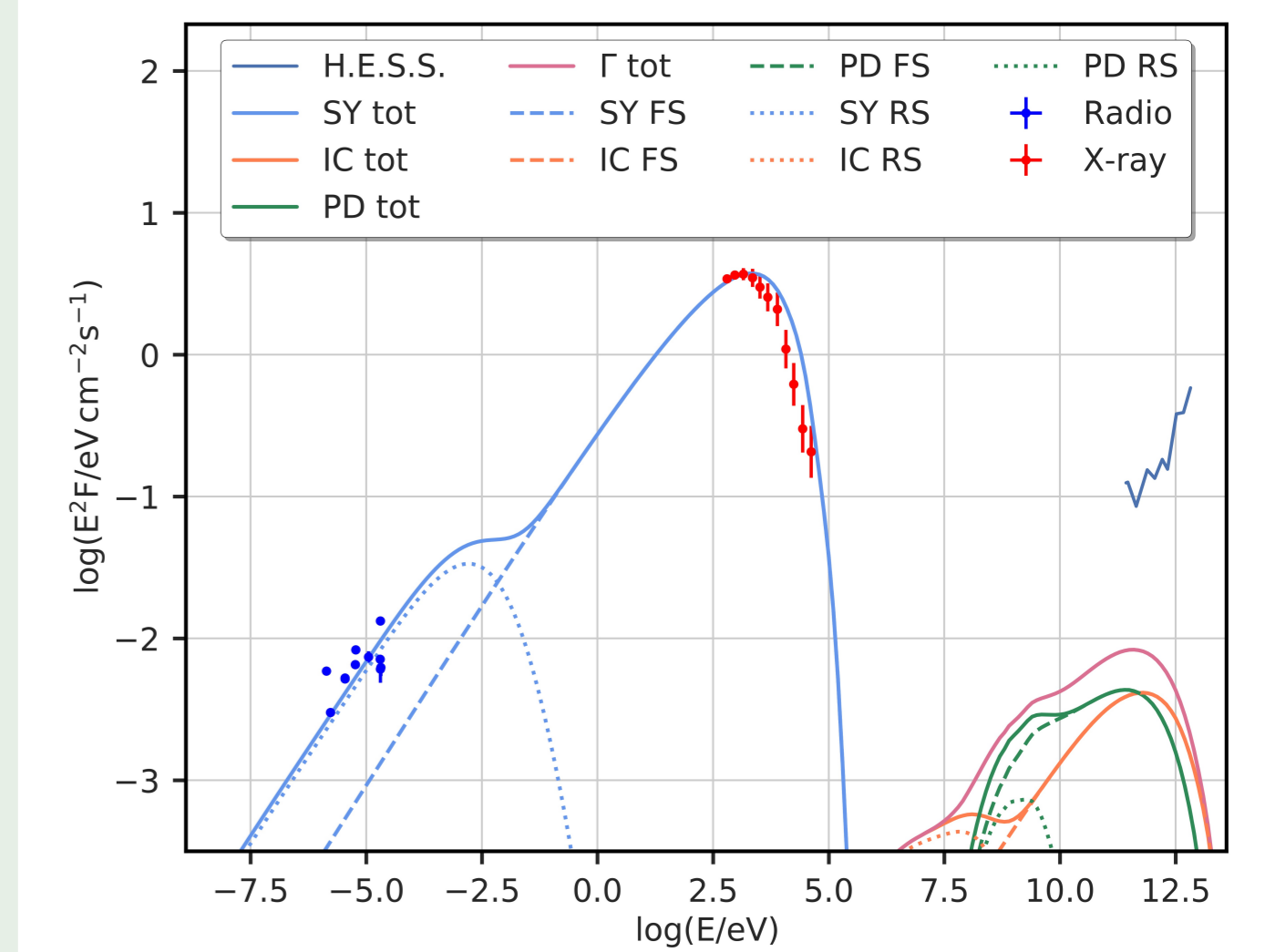


Figure: Combined SED of the forward (FS) and reverse shock (RS) contributions.

4. Radio and x-ray brightening

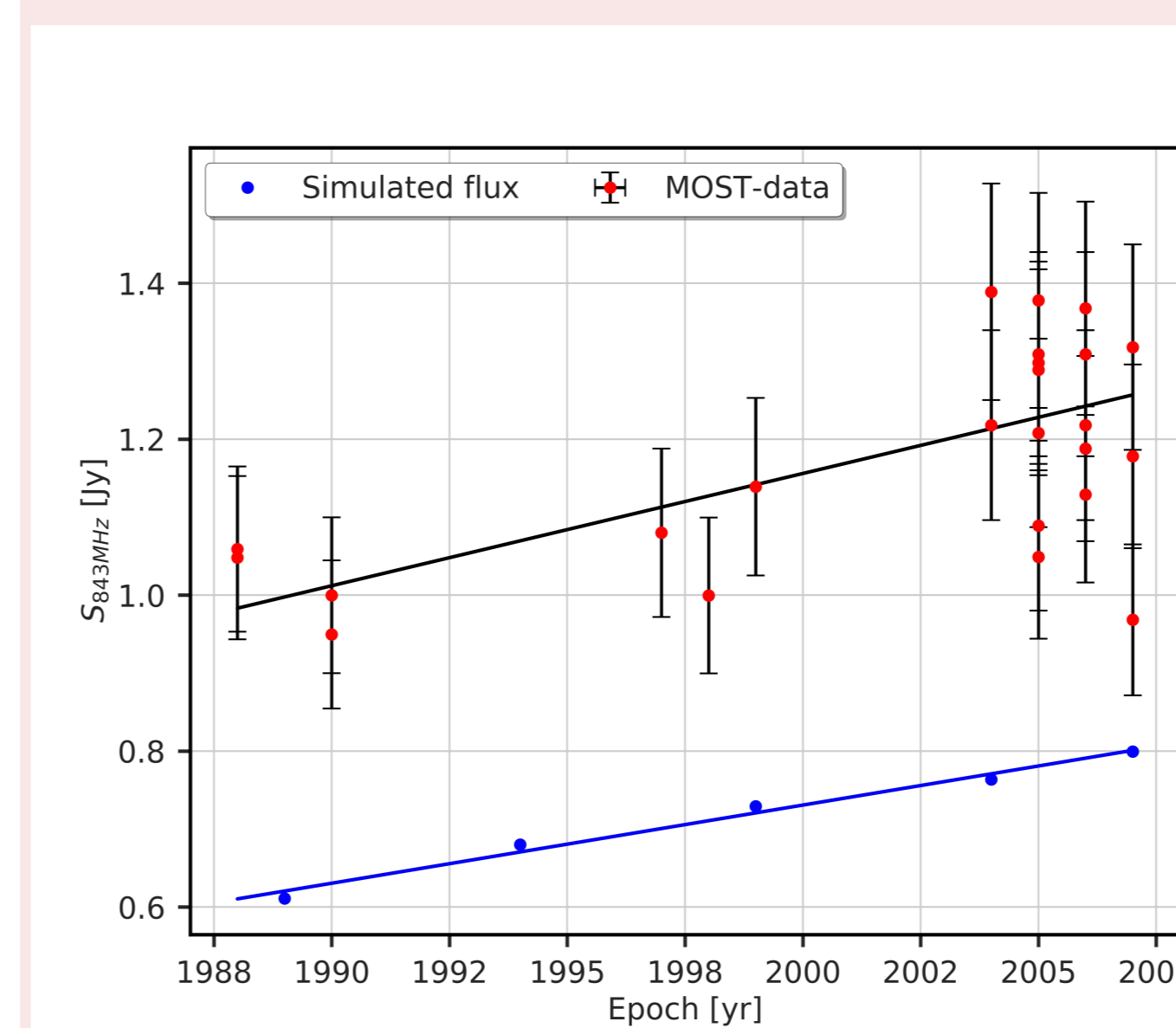


Figure: Evolution of the radio flux at 843 MHz. We reproduce the right order of magnitude for the radio flux as seen in section 2 but systematically undershoot the MOST-observations.

The radio brightening of the remnant depends mainly on the evolution of the magnetic field strength and the number of available electrons to radiate.

As the shock surface increases and thus the number of particles that can radiate increases, a radio brightening is expected even without changes in the magnetic-field strength. The relative increase in the number of particles is 1.9%/yr for the forward shock and 1.6%/yr for the reverse shock.

In our model, we obtain a flux increase of 1.64%/yr, which is in good agreement with the 1.2%/yr observed for the radio flux [8].

For the x-ray flux, we obtain a value of 1.8%/yr which is well in agreement with the 1.9%/yr increase measured by Chandra [9].

5. Prospects for CTA

The gamma-ray emission from G1.9+0.3 is dominated by inverse Compton scattering of the high energetic electrons accelerated at the forward shock on CMB and IR photons. Our predictions for the gamma-ray emission are well in agreement with the H.E.S.S. upper limits and about three times below the proposed sensitivity of CTA south. Further we expect the gamma-ray flux to increase by about 25% in the epoch between 2007 and 2032.

Still there are good prospects of seeing a 3 sigma signal of G1.9+0.3 within about 170 hours of CTA observations.

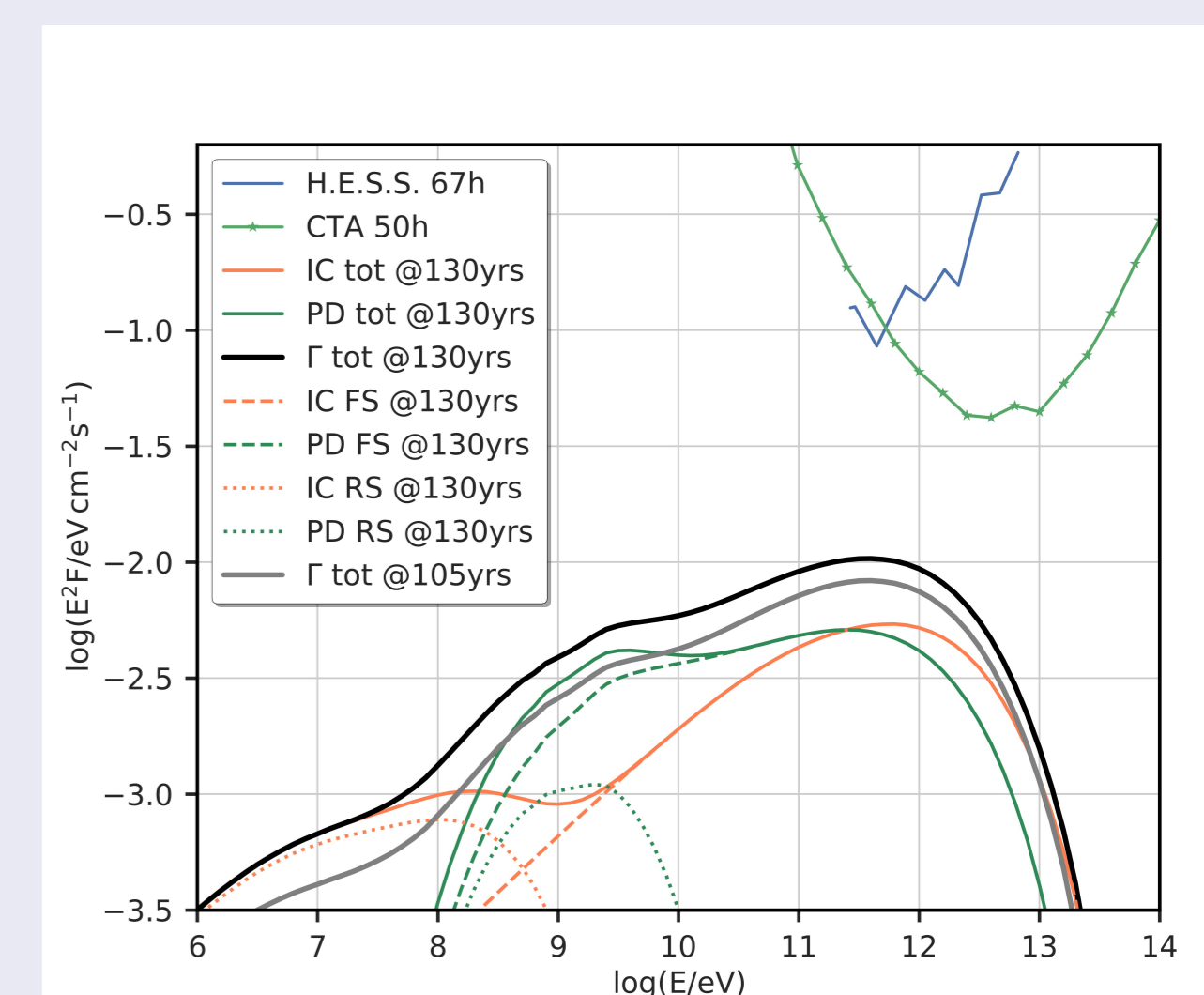


Figure: Gamma-ray emission from G1.9+0.3 in 2007 and 2032.

- A two shock scenario can explain the observed emission within the test-particle limit and moderate magnetic fields
- The separation between the x-ray and radio peaks in the East-West direction can be better explained with a two-shock scenario than a single-shock scenario
- The origin of x-ray and radio emission from different shocks allows to explain the different morphologies
- Our simulations reproduce the observed rates of radio and x-ray brightening
- G1.9+0.3 might be detectable by CTA south

Contact: robert.brose@desy.de

[1] I. Telezhinsky, V. V. Dvarkadas, and M. Pohl. Particle spectra from acceleration at forward and reverse shocks of young Type Ia Supernova Remnants. *Astroparticle Physics*, 35:300–311, January 2012.

[2] I. Telezhinsky, V. V. Dvarkadas, and M. Pohl. Time-dependent escape of cosmic rays from supernova remnants, and their interaction with dense media. *Astronomy and Astrophysics*, 541:A153, May 2012.

[3] I. Telezhinsky, V. V. Dvarkadas, and M. Pohl. Acceleration of cosmic rays by young core-collapse supernova remnants. *aap*, 552:A102, April 2013.

[4] R. Brose, I. Telezhinsky, and M. Pohl. Transport of magnetic turbulence in supernova remnants. *aap*, 593:A20, August 2016.

[5] A. Mignone, G. Bodo, S. Massaglia, T. Matsakos, O. Tesileanu, C. Zanni, and A. Ferrari. PLUTO: A Numerical Code for Computational Astrophysics. *apjs*, 170:228–242, May 2007.

[6] V. V. Dvarkadas and R. A. Chevalier. Interaction of Type Ia Supernovae with Their Surroundings. *apj*, 497:807–823, April 1998.

[7] K. J. Borkowski, P. Gwynne, S. P. Reynolds, D. A. Green, U. Hwang, R. Petre, and R. Willett. Asymmetric Expansion of the Youngest Galactic Supernova Remnant G1.9+0.3. *Astrophysical Journal Letters*, 837:L7, March 2017.

[8] T. Murphy, B. M. Gaensler, and S. Chatterjee. A 20-yr radio light curve for the young supernova remnant G1.9+0.3. *Monthly Notices of the RAS*, 389:L23–L27, September 2008.

[9] K. J. Borkowski, S. P. Reynolds, D. A. Green, U. Hwang, R. Petre, K. Krishnamurthy, and R. Willett. Nonuniform Expansion of the Youngest Galactic Supernova Remnant G1.9+0.3. *Astrophysical Journal Letters*, 790:L16, August 2014.

